Photonics applications II

- ✓ Ion-doped ChGs

- Important
- Condensed summary

ChG as a host for doping; pros and cons

- ✓ Low phonon energy;
  - ➢ Enabling emission at longer wavelengths
  - ➢ Reduced nonradiative multiphonon relaxation
  - ➢ Relatively weak thermal stability
- ✓ High refractive index;
  - ➢ Enhancement in spontaneous emission rate and absorption cross-section
  - ➢ Relatively strong optical confinement
  - ➢ Poor optical coupling due to large refractive index difference
- ✓ Small band gap energy;
  - ➢ Excitation via host sensitization
  - ➢ Pump energy loss due to two photon absorption
- ✓ Large optical nonlinearity
  - ➢ Provide a good opportunity?
  - ➢ Limits in increasing pumping power

RE-doped glasses

- ✓ Radiative emissions in the IR wavelengths; compared to those of transition metal ions
  - ➢ Mostly (ED- and/or MD-induced) 4*f*-4*f* transitions
  - ➢ Not much sensitive to the local fields, i.e., host compositions
  - ➢ Relatively small absorption and emission cross sections

- ✓ Relatively narrower spectral coverage in general

- ✓ Numerous RE-host combinations

- ✓ From fundamental spectroscopy to commercialized modules; High-power fiber laser, EDFA…

Important parameters for evaluation

- ✓ With respect to dopant, spectroscopic properties;
  - ➢ Spectral coverage and branching ratio
  - ➢ Measured lifetime and quantum efficiency
  - ➢ Absorption and emission cross-sections
  - ➢ Position in energy of the fluorescing manifold
  - ➢ Pump and signal excited-state absorptions
  - ➢ Radiative and nonradiative energy transfers
- ✓ With respect to host;
  - ➢ Thermal stability and feasibility of waveguide fabrication
  - ➢ Rare-earths solubility and concentration quenching
  - ➢ Optical loss of a waveguide
  - ➢ Optical nonlinearity
  - ➢ Mechanical/chemical properties and long term durability
  - ➢ Something that we still don’t know

Energy levels of *4f* configuration of RE

Emission at longer wavelength from transition between levels of narrow energy separation

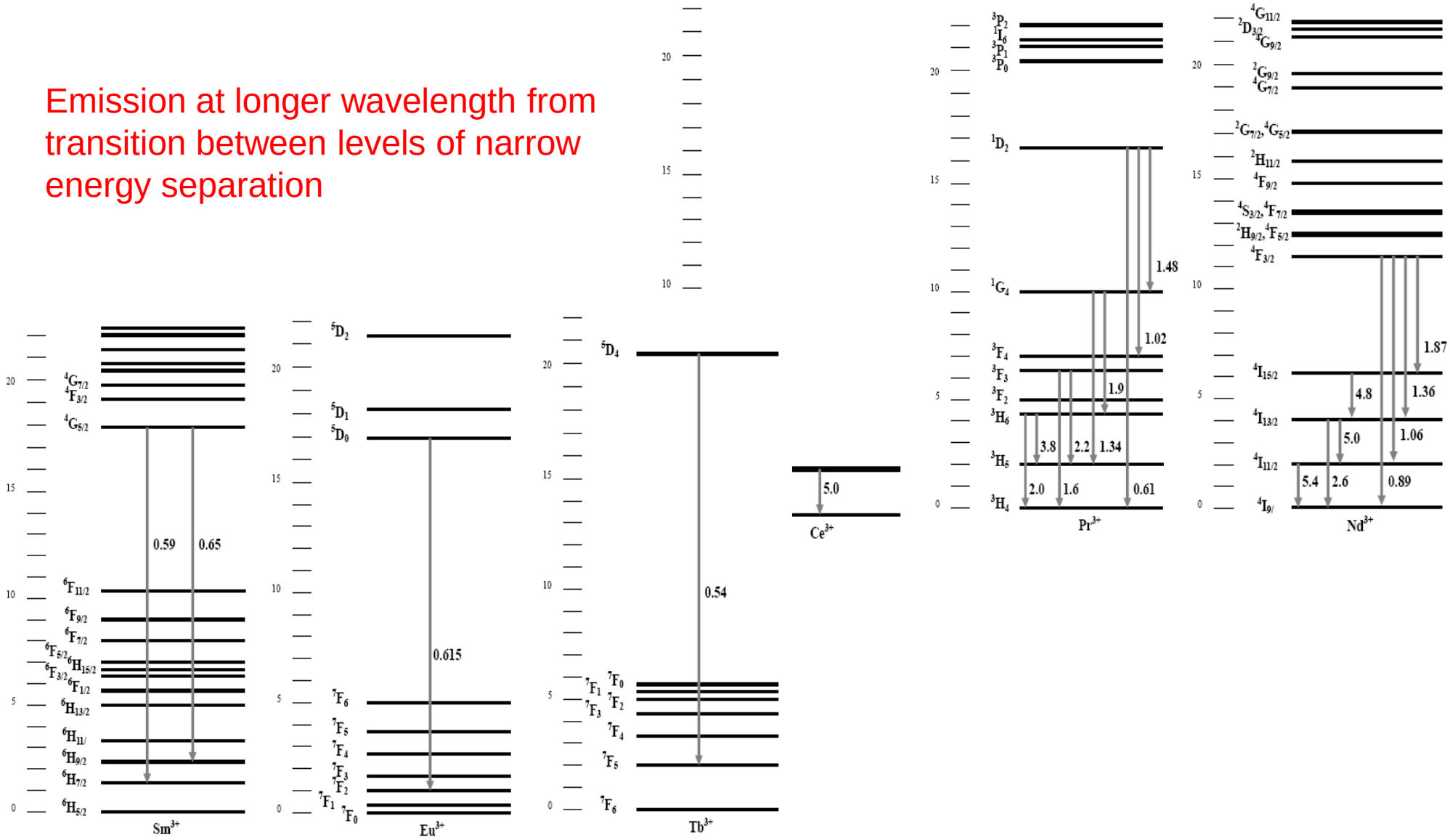

Energy levels of *4f* configuration of RE

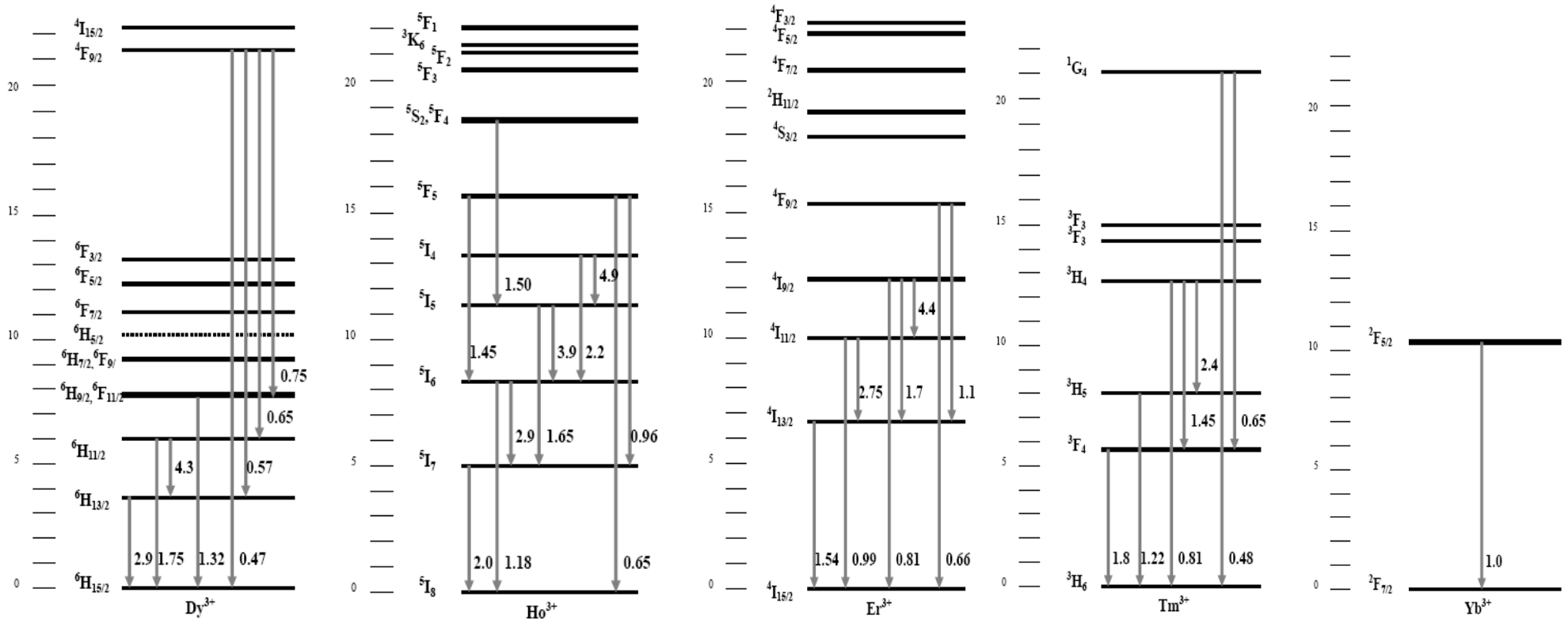

- Important
- Needs understanding

Spontaneous or stimulated

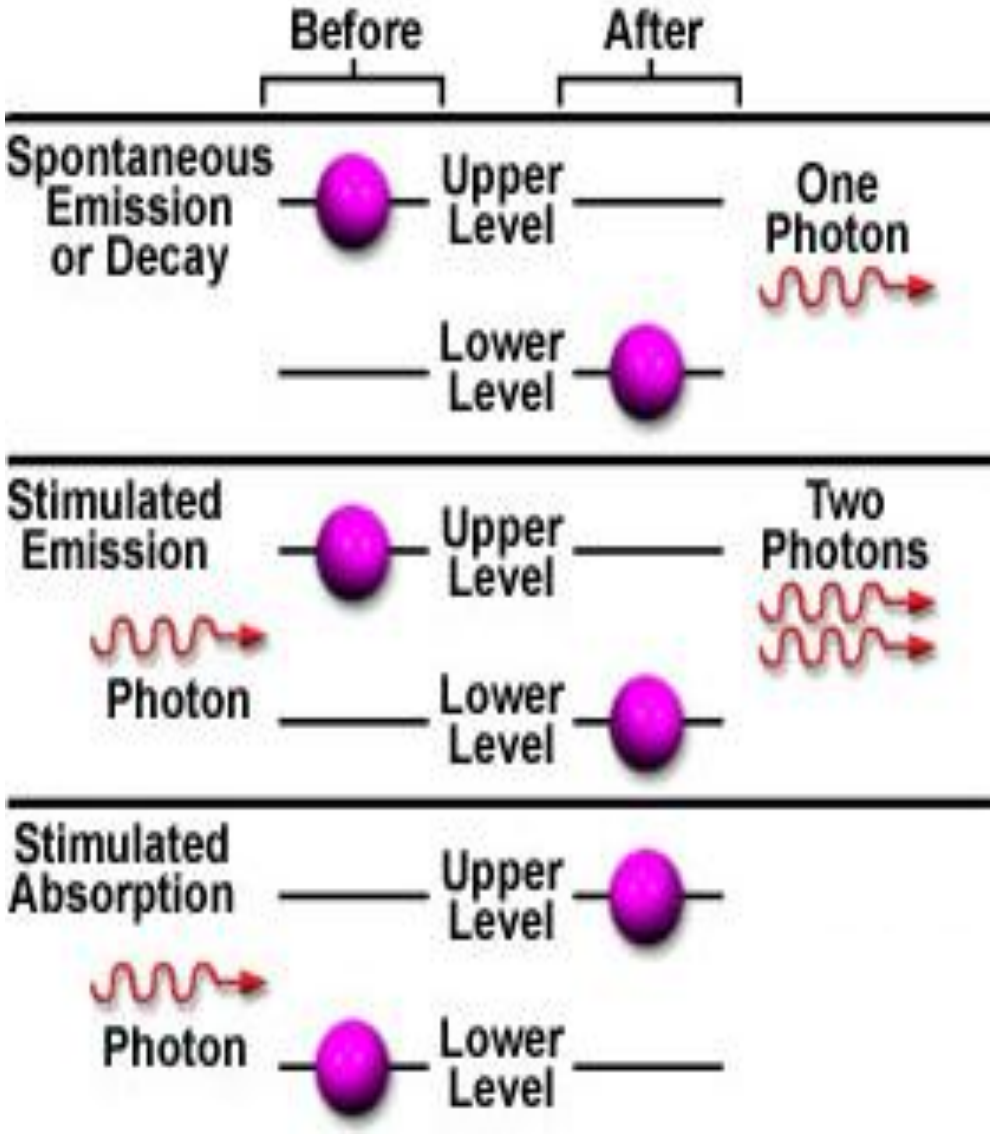

- ✓ Spontaneous emission rate
  - ➢ Intrinsic lifetime
- ✓ Incoherent light source;
  - ➢ Fluorescent lamps
  - ➢ LED

- ✓ Stimulated emission cross section
- ✓ Coherent light source;
  - ➢ Laser

- ✓ (Stimulated) absorption cross section

* Figure from http://micro.magnet.fsu.edu/primer/java/lasers/electroncycle/index.html

Spontaneous emission rate (SER)

$$\Gamma_0 = \frac{1}{\tau_0} = \frac{2\pi}{\hbar}\left\langle \left| E_{sp}^{loc} \cdot \mu_{01} \right|^2 \right\rangle_{osc} \rho(\omega)$$

- ✓ Spontaneous emission must occur if matter and radiation are to achieve thermal equilibrium (vacuum fluctuation).
  - ➢ Amplitude of the local electric field oscillations E_{sp}^{loc}
  - ➢ Electric dipole moment μ_{01}
  - ➢ Density of the electromagnetic field oscillators $\rho(\omega)$

- ✓ SER can be modified by changing the environments.
  - ➢ **Local fields effect of a host medium**
  - ➢ Purcell effect in optical cavities
  - ➢ Photonic bandgap effect in spatially inhomogeneous dielectrics

Intra-4*f*-configurational transitions of RE

- ✓ Oscillator strength (experimental)
  - ➢ Absorption cross-section spectrum

$$f = 4\pi\varepsilon_0 \frac{mc^2}{\pi e^2} \int \sigma(\nu)\, d\nu$$

- ✓ Oscillator strength (theoretical)
  - ➢ Electric-dipole line strength
  - ➢ Local field correction factor

$$f(a;b) = \frac{\ell^2}{n} \frac{1}{g_a} \frac{8\pi^2 mc\nu_0}{3he^2} S_{ed}(a;b)$$

- ✓ Electric-dipole line strength
  - ➢ Judd-Ofelt intensity parameters
  - ➢ Doubly reduced tensor matrix

$$S_{ed}(a;b) = e^2 \sum_{t=2,4,6} \Omega_t \left\langle a \left\| U^{(t)} \right\| b \right\rangle^2$$

- ✓ Spontaneous emission rate
  - ➢ Electric-dipole line strength
  - ➢ Local field correction factor

$$\Gamma = A_{ed}(bJ';aJ) = \frac{1}{4\pi\varepsilon_0} \frac{64\pi^4}{3h(2J'+1)\lambda^3} \ell^2 n S_{ed}$$

* B.R. Judd, *Phys. Rev.* 127 (1962) 750.
* G.S. Ofelt, *J. Chem. Phys*. 37 (1962) 511.

Controlling SER

- ✓ **Adjust the local electrical fields and/or the line strengths**
  - ➢ **Via refractive index and/or local atomic arrangements**

- ✓ SER of dipole emitter embedded in a homogeneous medium is changed;

$$\Gamma = \ell^2 \varepsilon_r^{0.5} \Gamma_0$$

  - ➢ The local fields correction problem arises.
- ✓ The virtual-cavity model (Lorentzian local field correction);

$$\ell = \frac{\varepsilon_r + 2}{3}$$

- ✓ The real-cavity model;

$$\ell = \frac{3\varepsilon_r}{2\varepsilon_r + 1}$$

* Toptygin, J. Fluores. 13 (2003) 201.

Effects of the local fields

- ✓ Refractive index does affect absorption and emission by way of the local fields effect.
- ✓ Care should be paid when applying the local fields correction.
- ✓ Further experimental evaluation is needed to confirm which correction is more suitable for the ChGs.

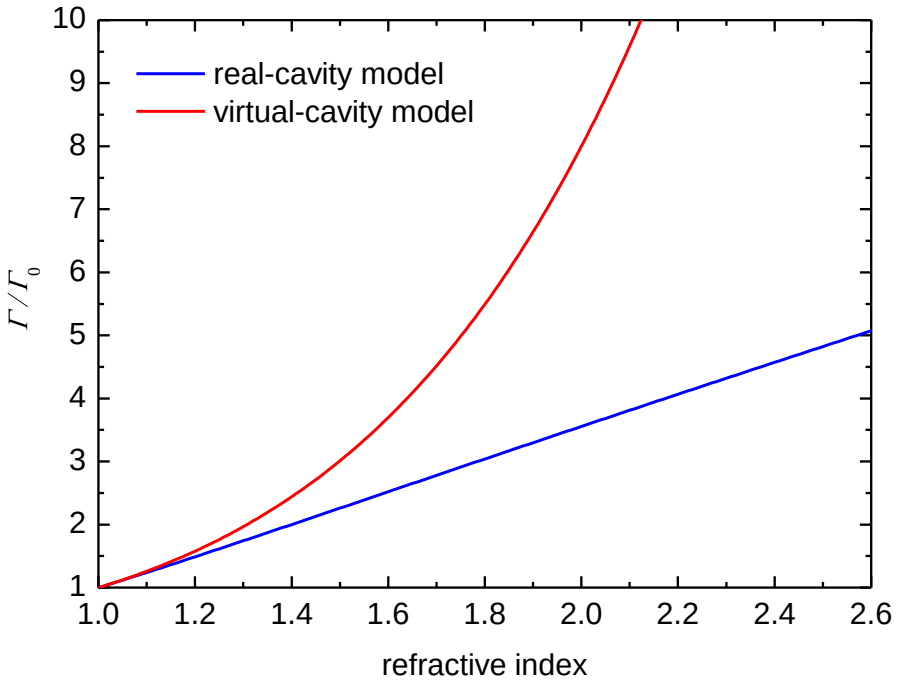

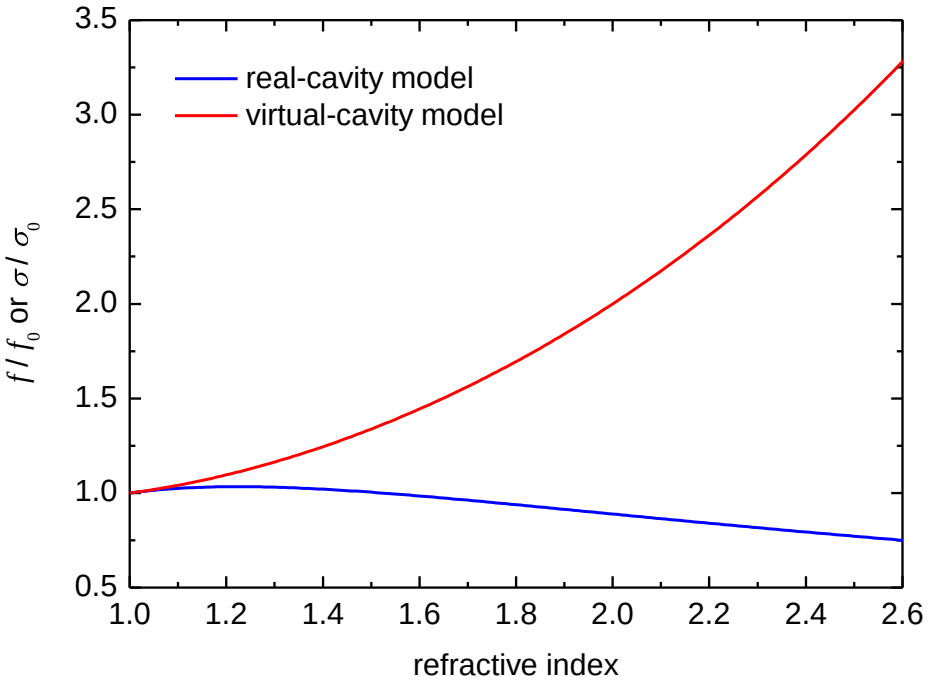

* Choi and Song, Chem. Phys. Lett. 467 (2009) 323.

Parameters involved in measured decay rate

For emitters embedded in dielectrics,

$$W_r = \tau_r^{-1}$$

$$W = \tau_m^{-1} = W_r + W_{nr} = W_r + W_{MP} + W_{ET} + W_{CR} - W_{RT}$$

τ_r : radiative lifetime, i.e., the reciprocal of spontaneous emission rate

τ_m : measured lifetime

W_{MP} : quenching due to multiphonon relaxation

W_{ET} : quenching due to ion-impurity interaction

W_{CR} : quenching due to ion-ion interaction (cross-relaxation)

W_{RT} : virtual increase owing to radiation trapping

Quantum efficiency: τ_m/τ_r

Multiphonon relaxation

✓ Phenomenological energy gap law;

$$W_{MP} = W_0 \exp(-\alpha \Delta E)$$

ΔE : energy gap to the next-lower-lying level

α : parameter inversely proportional to phonon energy

✓ Radiation and phonon relaxation: **a competing process**

✓ Energy can be transformed into heat as a result of MPR.

Low phonon energy hosts

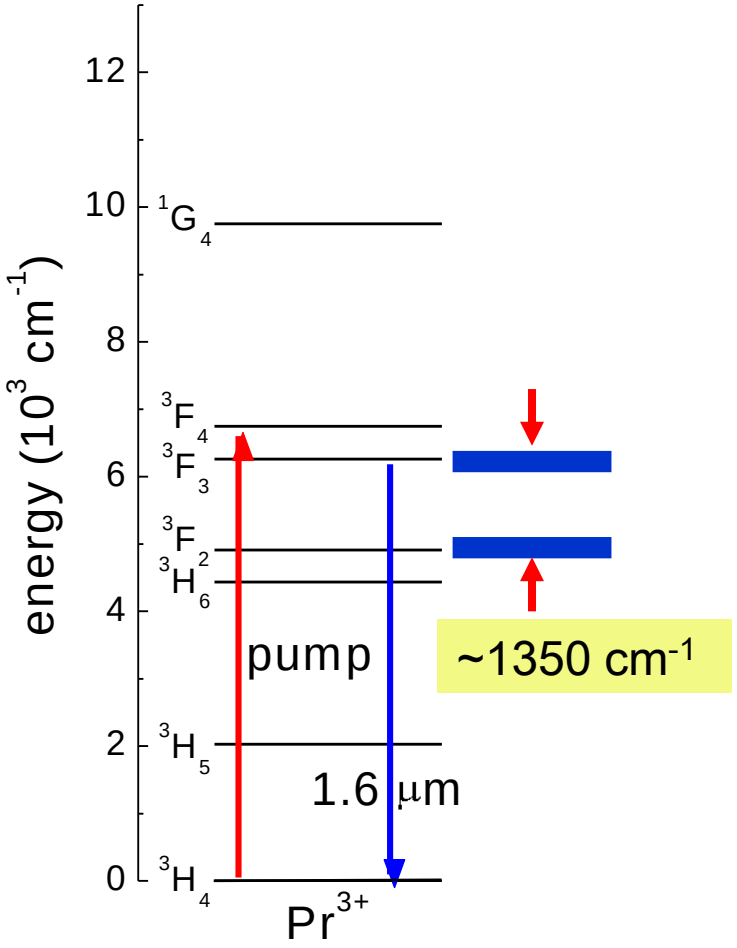

Glass	Phonon energy cm^{-1}	1.6 μm emission
Silica	~1100	No
Tellurite	~700	No
Fluoride	~500	No
Sulfide	~350	No
Selenide	~200	Yes

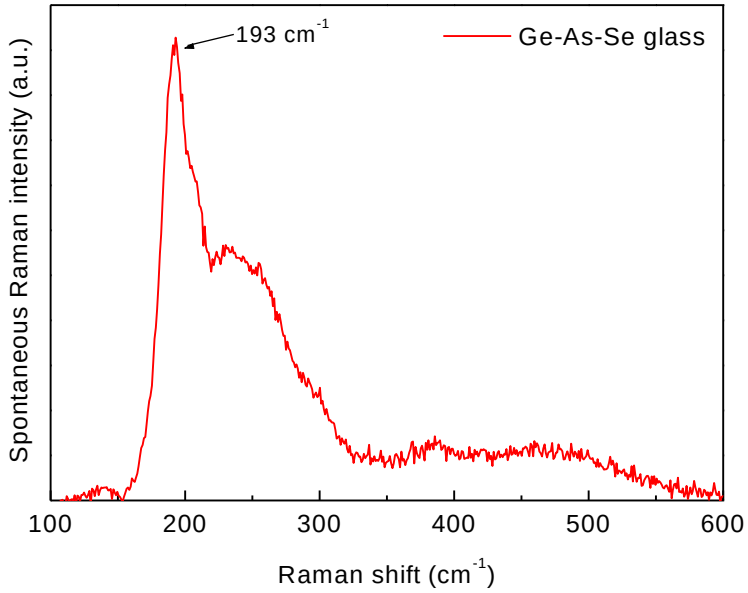

* Choi et al, Appl. Phys. Lett. 78 (2001) 1249.

Improved light emission

✓ Due to decreased MPR

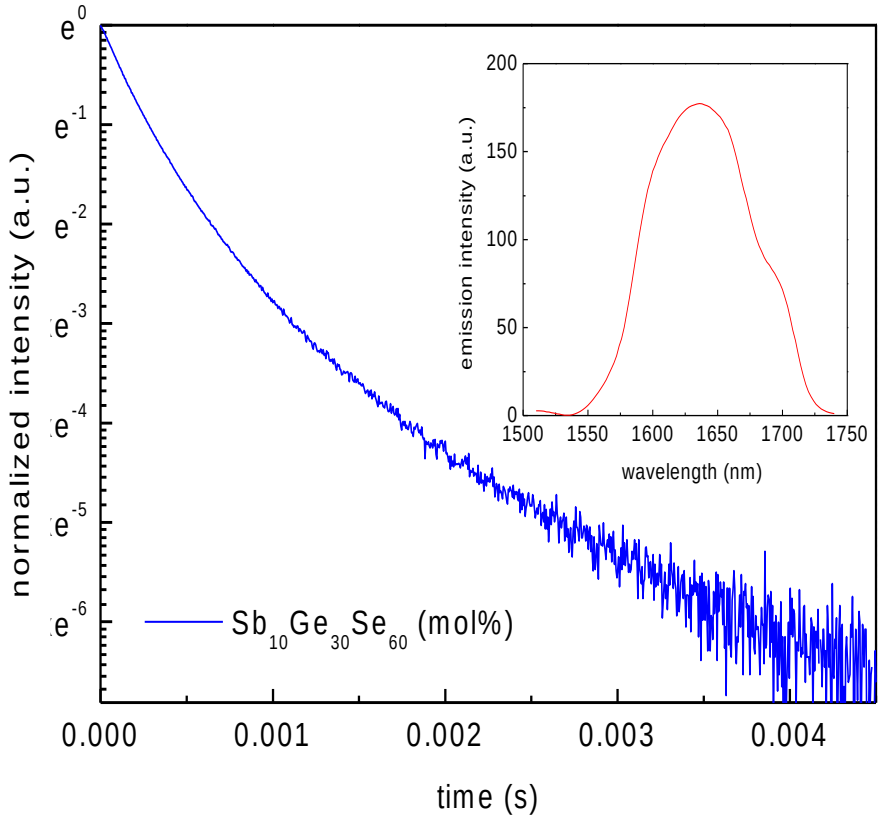

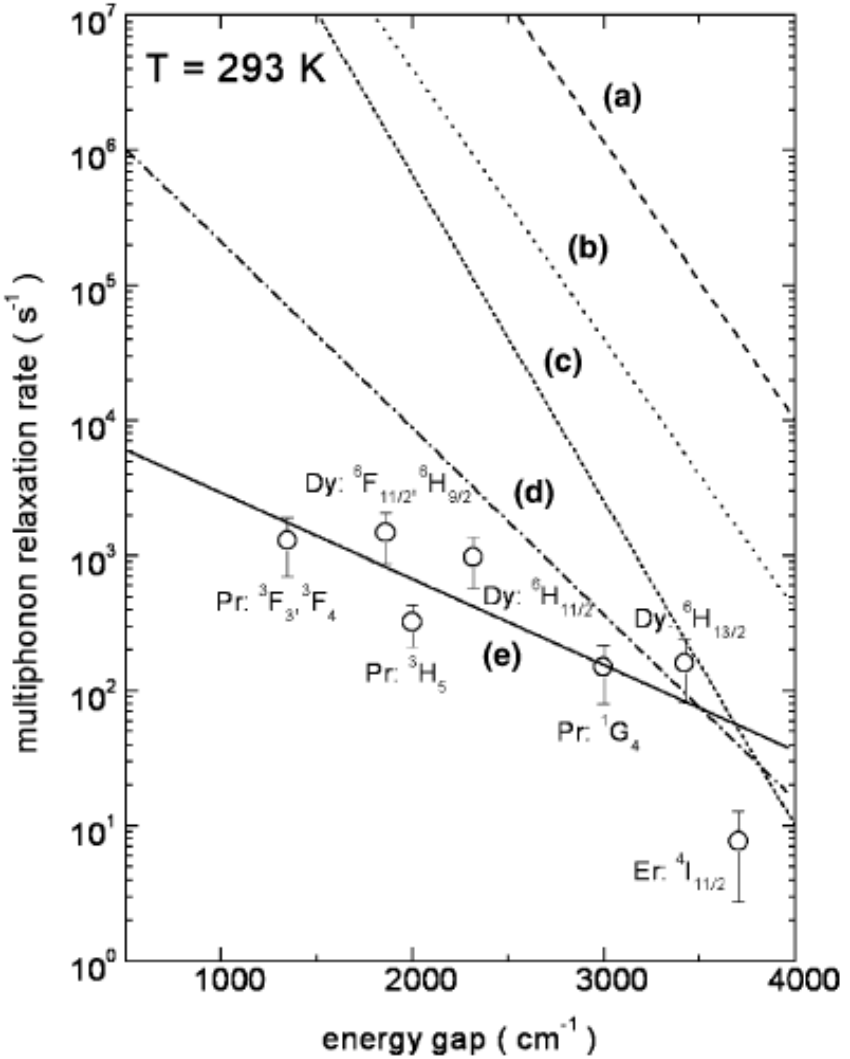

Fig. 4. Multiphonon relaxation rates for (a) silicate, (b) tellurite, (c) fluoride, (d) Ga–La (or Al)–S, and (e) $Ge_{30}As_8Ga_2Se_{60}$ glasses. Note that the lines for the glasses except for selenide are drawn according to the respective data in [18].

* Choi et al, ETRI J. 23 (2001) 97.

* Choi et al, Chem. Phys. Lett. 368 (2003) 625.

RE-doped ChG; Nd^{3+}: 1.06 μm emission

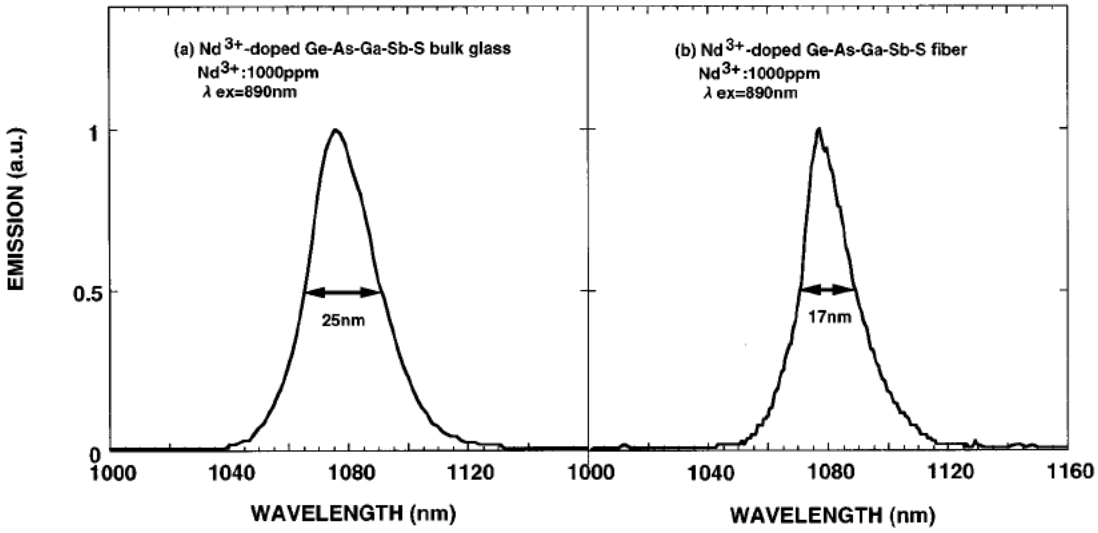

FIG. 4. Emission spectra from (a) the Nd^{3+}-doped chalcogenide bulk glass and (b) the fiber as a result of the ${}^4F_{3/2}-{}^4I_{13/2}$ transition.

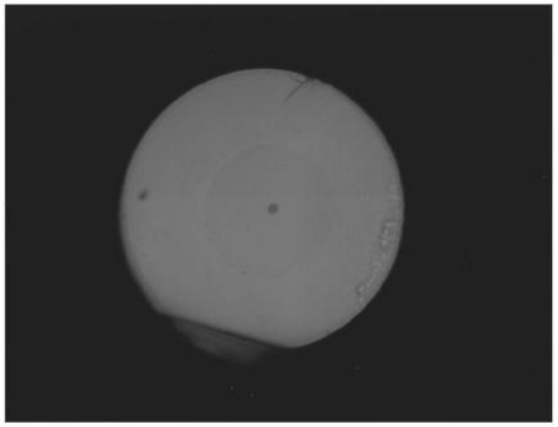

FIG. 2. An optical micrograph of a fiber cross section. The fiber has a thin core diameter of 5 μm and a cladding diameter of 120 μm.

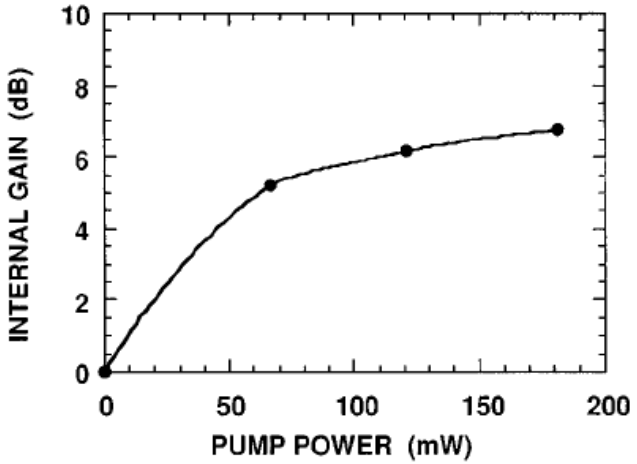

FIG. 5. The pump power dependence of the internal gain of Nd^{3+}doped chalcogenide fiber. The input signal power and the fiber length are −30 dBm and 5 cm, respectively.

* Mori et al, Appl. Phys. Lett. 70 (1997) 230.

RE-doped ChG; Nd^{3+}: 1.06 μm emission

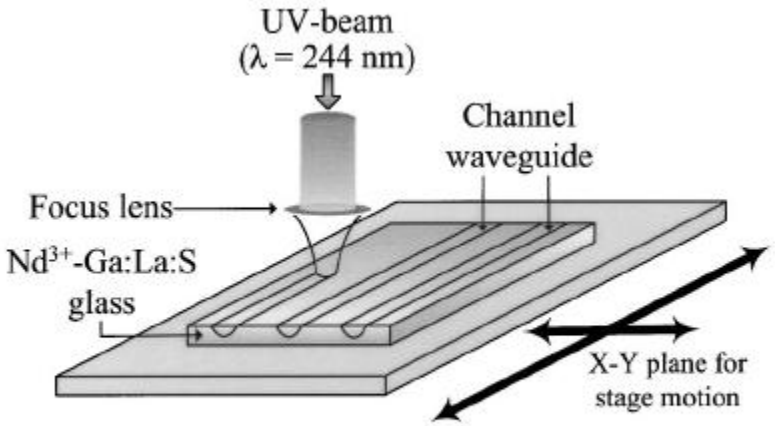

FIG. 1. Schematic diagram of the setup used to directly write channel waveguides into Nd^{3+} – Ga:La:S bulk glass.

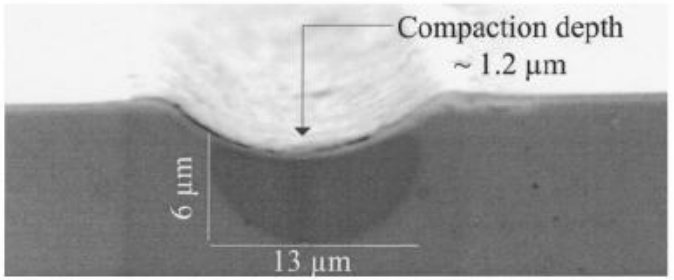

FIG. 2. Micrograph (SEM) of a channel waveguide written with laser fluence of 10.8 J/cm^2. Surface compaction is 1.2 μm and physical channel size of 13 μm by 6 μm is shown.

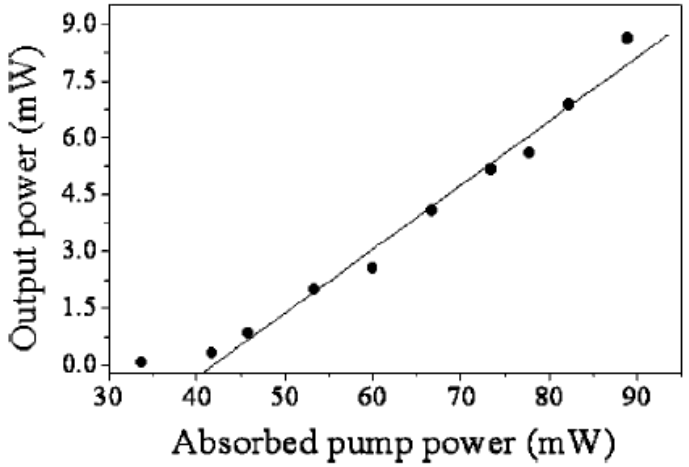

FIG. 3. Peak output power of 8.6 mW for 89 mW of absorbed pump power and slope efficiency of 17% with the upper limit of waveguide attenuation <0.5 dB cm^{-1}.

* Mairaj et al, Appl. Phys. Lett. 81 (2002) 3709.

RE-doped ChG; Pr^{3+}: 1.3 μm emission

- ✓ Demonstration of sulfide-based fiber amplifier*
  - ➢ Pr^{3+}-doped sulfide Ga-Na-S system
  - ➢ A singlemode fiber with attenuation loss of 1.2 dB/m at 1.31 μm
  - ➢ Bidirectional pumping at 1020 nm
  - ➢ Gain coefficient of 0.81 dB/mW at a wavelength of 1.34 μm
  - ➢ A net gain of 32 dB for a pump power of 90 mW
  - ➢ Lifetime of $^1G_4$ level; longer than 300 μs
- ✓ Sulfide glass fiber confirmed its practicality.

* Tawarayama et al, J. Am. Ceram. Soc. 83 (2000) 792.

MIR emission from RE^{3+}-doped selenide glasses

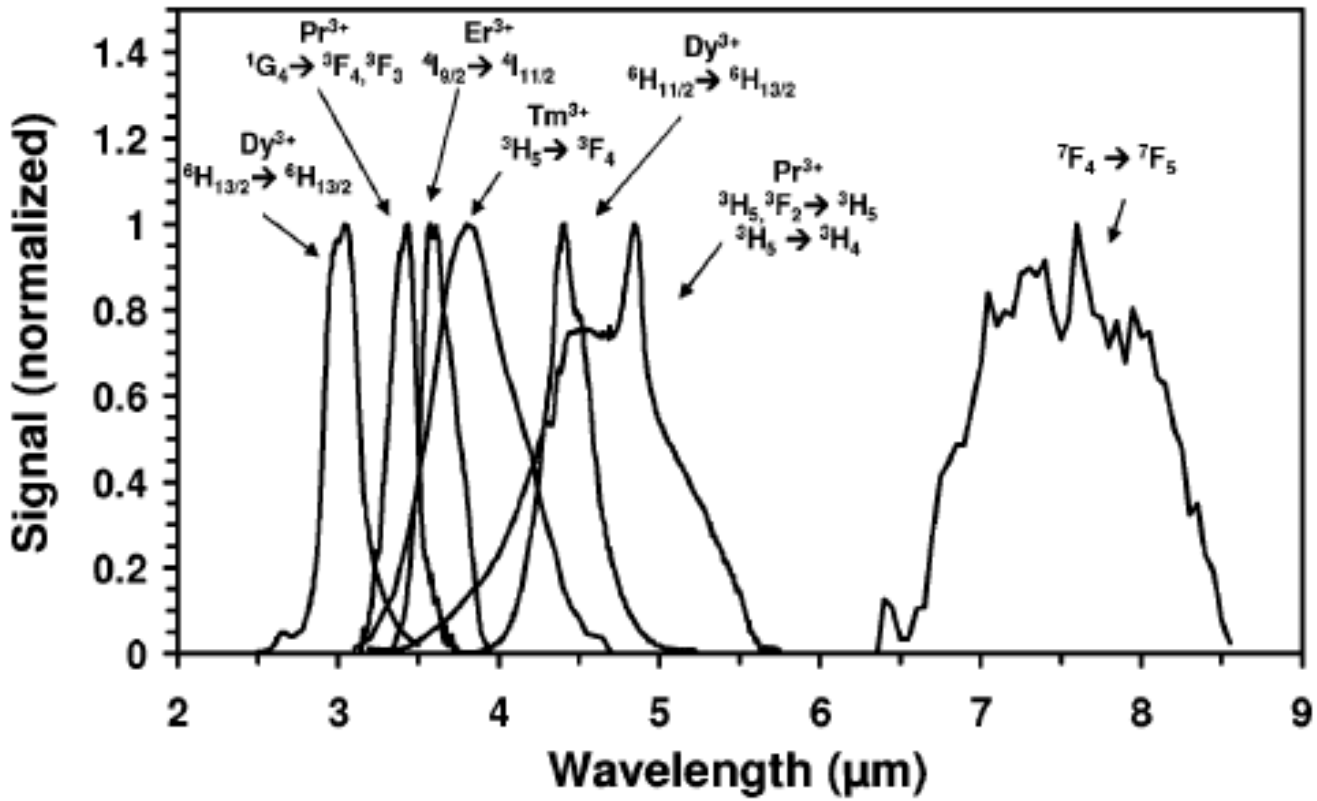

Fig. 4. Rare-earth-doped chalcogenide (Ge–As–Ga–Se) glass IR transitions within the 2–5 μm atmospheric transmission window. Also shown is the $\sim$8 μm transition of Tb^{3+}.

* Sangehera et al, IEEE J. SELECTED TOPICS IN QUANTUM ELECTRONICS, 15 (2009) 114.

MIR emission from RE^{3+}-doped selenide glasses

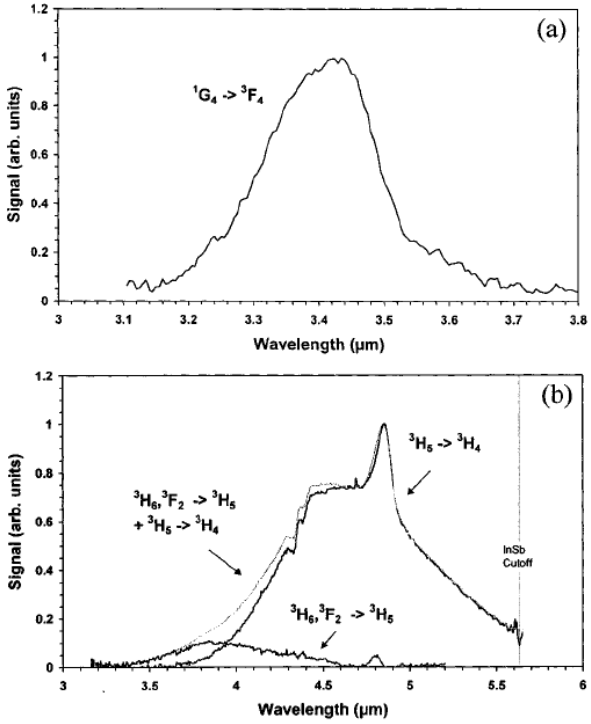

Fig. 5. Room-temperature fluorescence spectra of the MWIR transitions in Pr^{3+}. (a) $^1G_4 \rightarrow {}^3F_4$ uncorrected fluorescence spectra. (b) The 3–5-μm emission from the ($^3H_6$, $^3F_2$) and $^3H_5$ levels in Pr^{3+}-doped GAGSe under 1.97-μm pumping. The contribution from the ($^3H_6$, $^3F_2$) $\rightarrow$ $^3H_5$ and $^3H_5 \rightarrow {}^3H_4$ transitions are shown in grey.

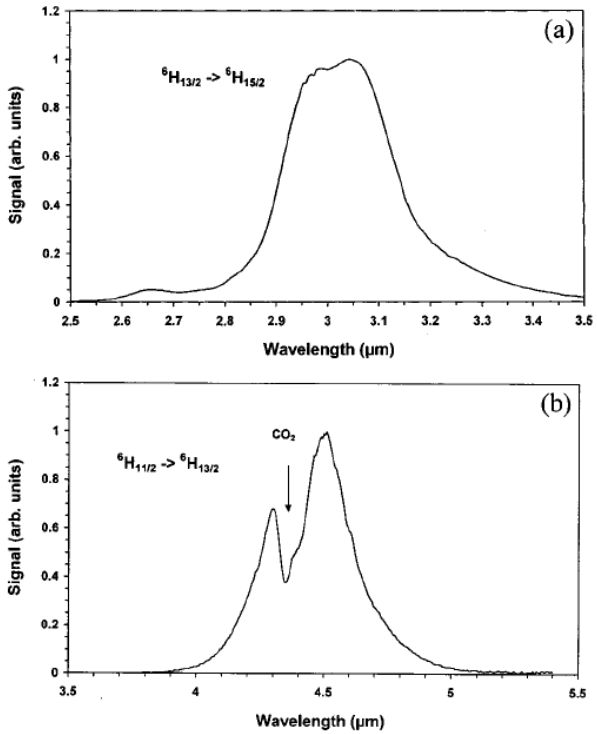

Fig. 9. Room-temperature fluorescence spectra of the MWIR transitions in Dy^{3+}. (a) $^6H_{13/2} \rightarrow {}^6H_{15/2}$ uncorrected fluorescence spectra. (b) $^6H_{11/2} \rightarrow {}^6H_{13/2}$ uncorrected fluorescence spectra. The dip at ~4.3 μm is due to atmospheric CO_2 absorption.

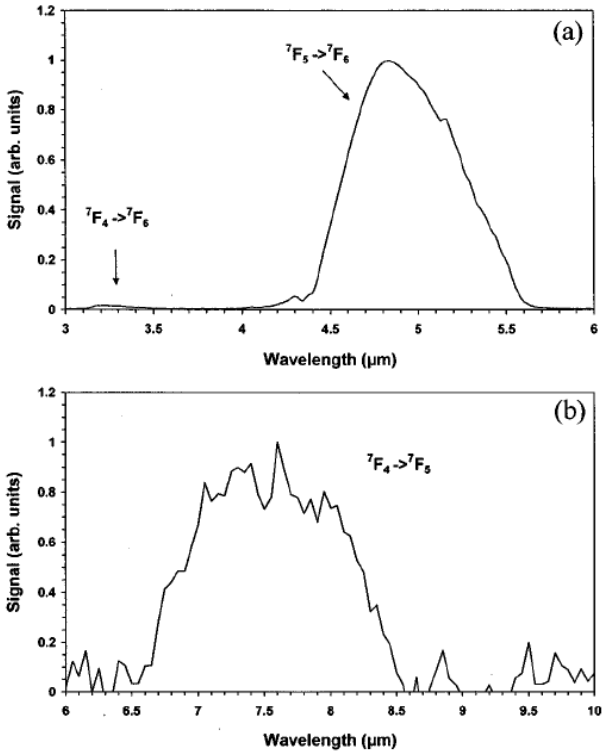

Fig. 13. Room-temperature fluorescence spectra of the MWIR and LWIR transitions in Tb^{3+}. (a) $^7F_5 \rightarrow {}^7F_6$ and $^7F_4 \rightarrow {}^7F_6$ uncorrected fluorescence spectra. (b) $^7F_4 \rightarrow {}^7F_5$ uncorrected fluorescence spectra.

* Shaw et al, IEEE J. QUANTUM ELECTRONICS, 48 (2001) 1127.

- Important

Table 1. Collation of the mid-IR emission of RE-ion doped bulk chalcogenide glasses, and fiber, at ≥ 3 μm wavelength. Glasses are in blocks according to their ionic or covalent behavior and the host-glass chalcogen. References are in date-order in each block. Key: - means data are not available.

Glass	Fiber or Bulk	RE-ion	RE-ion concn. /ppm	Output$_\lambda$ / μm	Experimental lifetime /ms	Quantum efficiency / %	Year	Comment	Ref.
'p-block' selenide glasses									
GeGaAsSe.	Fiber.	Dy^{3+}	($3x10^{19}$ ions cm^{-3})	4.6.	-	-	2010	Modeling.	[44]
GeGaAsSe.	Fiber.	Dy^{3+}	($7x10^{19}$ ions cm^{-3})	4.2-4.7.	-	-	2008	Modeling	[43]
GeGaAsSe.	Bulk.	Pr^{3+}	1000.	4.8, 4.0, 5.2, 7.0, 3.4.	12, 4.2, 0.25, 0.25, 0.22.	80, 100, 86, 86, 61.	2001	Absorption and emission spectra are shown.	[26]
	Bulk.	Dy^{3+}	1100.	3.0, 4.5, 5.5, 7.6, 3.2.	6, 2, 0.31. <0.025, <0.025,	97, 83, 82, <7, <7			
	Bulk.	Tb^{3+}	1000.	4.8, 3.1, 7.5, 4.7, 10.5.	11, 0.012, 0.012, - , -.	73, 0.15, 0.15, -, -.			
GeGaAsSe.	Fiber.	Pr^{3+}	200.	-	-	-	2000	Fiber loss is stated.	[48]
	Fiber.	Dy^{3+}	200.	-	-	-			
'selenide'.	Fiber.	Dy^{3+}	-	~4.5.	-	-	2000	Fiber loss spectrum	[49]
'selenide'.	Fiber.	Pr^{3+}	-	3.5-5.5.	-	-	1999	Emission spectrum	[22]
'p-block' sulfide glasses									
GeGaSbS.	PCF Fiber	Er^{3+}	10,000	4.45-4.65.	-	-	2009	Modeling	[45]
GeGaSbS.	Bulk.	Er^{3+}	500 -10,000.	4.5.	-	-	2008	Emission spectrum	[25]
	Bulk.	Er^{3+}	10,000.	~4.3-4.8.	0.72.	64.			
	Fiber.	Er^{3+}	1000.	4.5.	-	-			
GeAsS.	Bulk.	Dy^{3+}	2000	5.27, 4.38.	- , 0.73.	-, 32.8.	1996	-	[50]
GeGaS.	Bulk.	Dy^{3+}	5000	5.27, 4.38.	0.038, 1.13.	-, 38.4.			
ionic sulfide glasses									
GLS	Bulk	Er^{3+}	(1.57 mol%)	3.62, 4.53	0.1, 0.59.	0.3, 0.5.	1997	Emission spectra	[51]
GLS(O)	Fiber	Er^{3+}		3.62, 4.53	-, -.	-, -.			
GLS	Bulk	Hm^{3+}	($8.9x10^{18}$ ions cm^{-3})	3.9, 4.9.	-,-.	9, 1.	1999	*Ditto*	[52]
GLS	Bulk	Dy^{3+}	(0.65 mol% Dy_2S_3)	4.3.	1.3.	7.4.	1999	*Ditto*	[53]
GLS	Bulk	Tm^{3+}	($0.35x10^{20}$ ions cm^{-3})	3.88, 5.38	-, -.	3, 0.2.	1999	Emission spectra are shown except at 8.1μm.	[54]
	Bulk	Tb^{3+}	(0.2 and 1.5 mol% Tb_2S_3	4.8, 3, 8.1.	0.1, -, -.	0.6, -, -.			

What should be done to lase in mid-IR region using doped ChG fiber?

$$(g - a)L$$

* Seddon et al, Optics Express 18 (2010) 26704.

Solubility of RE in ChG

- ✓ For RE solubility, the weak covalence is better?
  - ➢ Less than 0.1 wt% in Ge-As-S
  - ➢ Up to 1.0 wt% in Ge-Ga-S
  - ➢ Longer Dy-S distance in Ge-Ga-S
  - ➢ Ga forming [GaS_4] units which prefer RE^{3+}

	EXAFS				XRD	
Sample	Dy−S length (Å)	Coordination number	Debye-Waller factor (Å^2)	*R*-factor	Dy−S length (Å)	Coordination number
Dy_2S_3	2.82 ± 0.01	7.5 (fixed)	0.010 ± 0.001	0.0016	2.83	7.5
GAS	**2.78 ± 0.01**	**6.7 ± 0.5**	**0.009 ± 0.001**	**0.0034**		
GGS	**2.83 ± 0.01**	**7.1 ± 0.6**	**0.010 ± 0.001**	**0.0048**		

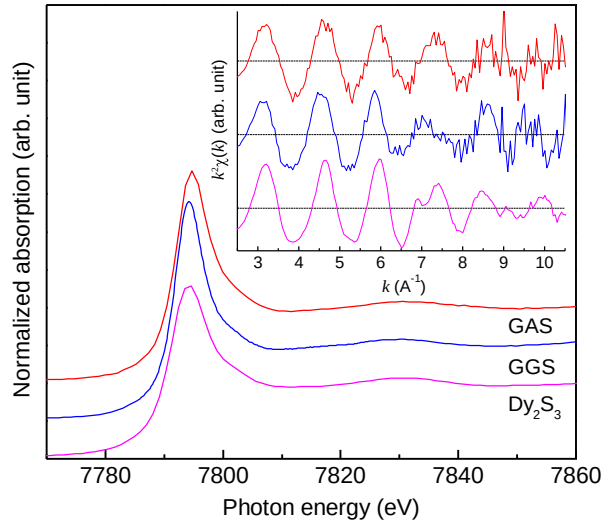

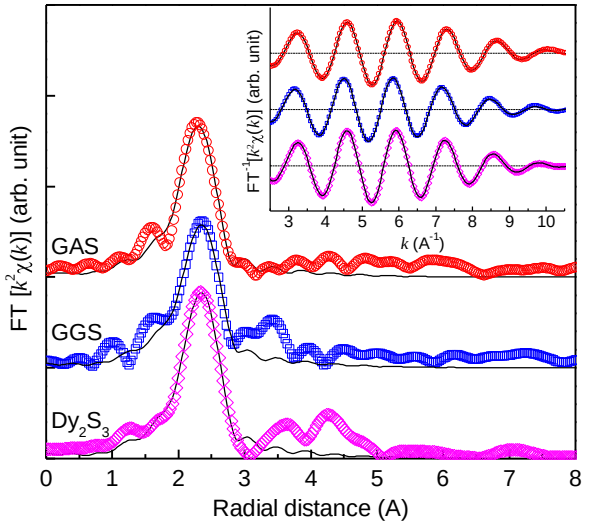

* Choi and Song, J. Non-Cryst. Solids 355 (2009) 2396.

Effects of host compositions

- ✓ The emission properties of Tm^{3+} in Ge–Ga–S glasses showed significant improvement with CsBr addition
- ✓ These changes in the emission properties are related to modification of the local environment of rare-earth ions upon CsBr addition

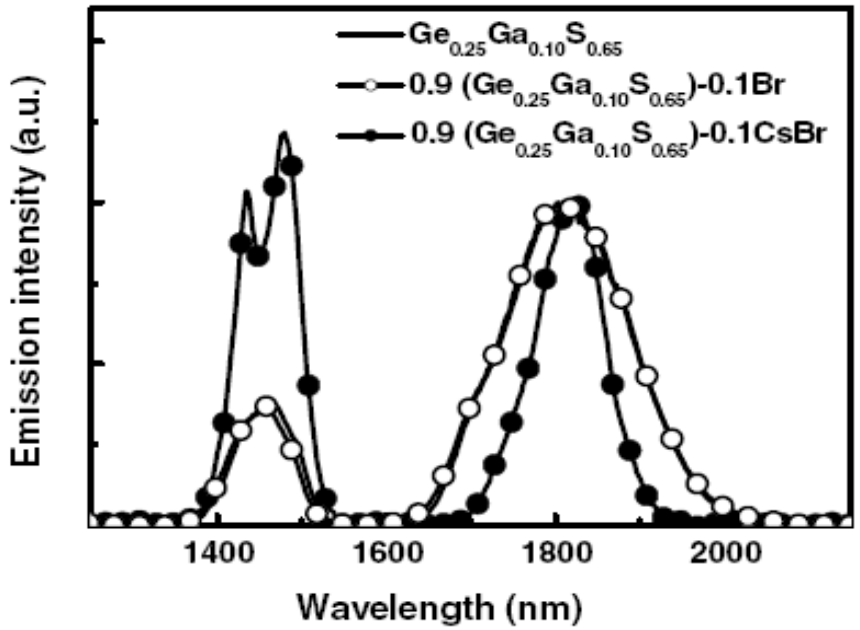

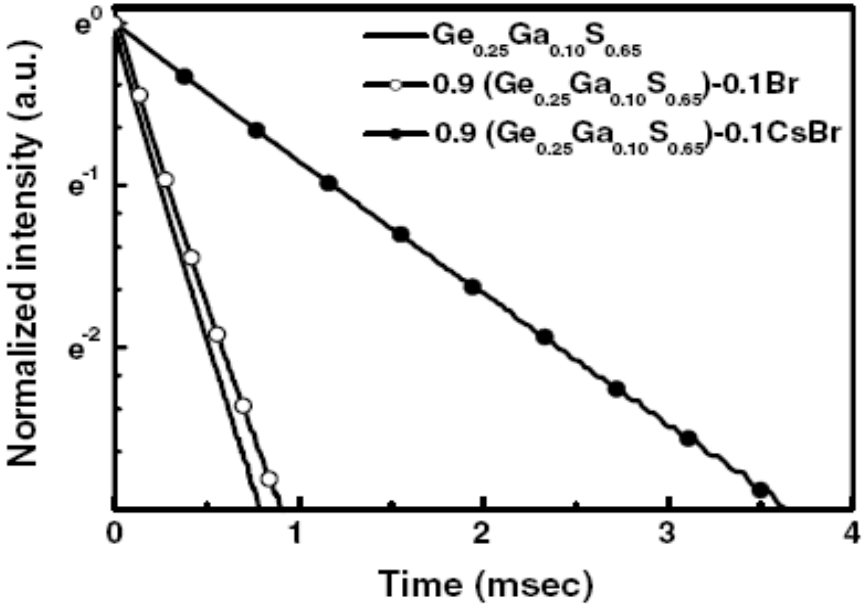

* Song et al, J. Non-Cryst. Solids 353 (2007) 1251.

Local structural changes; Tm L_3-edge EXAFS

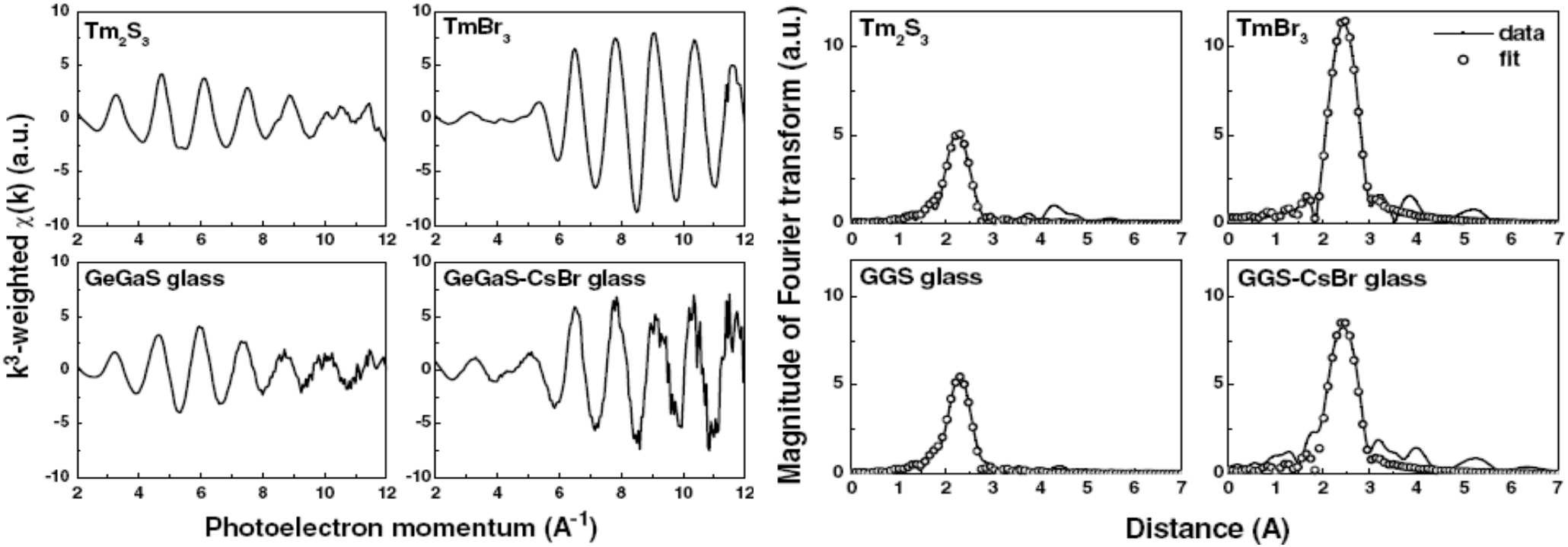

Coordination numbers (N), bond distances (R) and Debye–Waller factors (σ^2) of Tm–S and Tm–Br bonds in crystals and glasses, along with R-factors showing the validity of fitting

Bond	Composition	R (Å)	N	σ^2 (Å^2)	R-factor
Tm–S	Tm_2S_3 crystal	2.74 (0.01)	6.50 (fixed)	0.0115 (0.0015)	0.013
	$Ge_{0.25}Ga_{0.10}S_{0.65}$ glass	2.77 (0.01)	6.77 (0.85)	0.0107 (0.0014)	0.015
Tm–Br	$TmBr_3$ crystal	2.79 (0.01)	6.00 (fixed)	0.0066 (0.0003)	0.001
	0.90 ($Ge_{0.25}Ga_{0.10}S_{0.65}$) – 0.10CsBr glass	2.79 (0.01)	5.86 (1.58)	0.0083 (0.0018)	0.020

*Values in the parentheses are the estimated uncertainties.

* Song et al, J. Non-Cryst. Solids 353 (2007) 1251.

- For information

Dy^{3+}-doped Ge-As-S glass containing very small amounts of CsBr

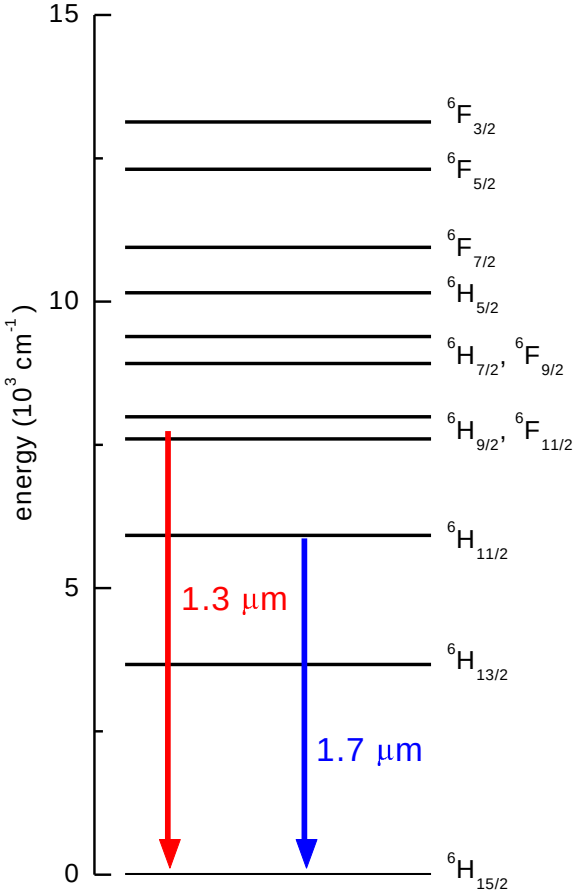

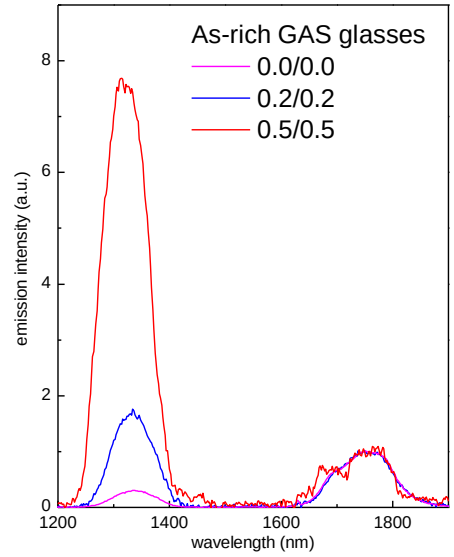

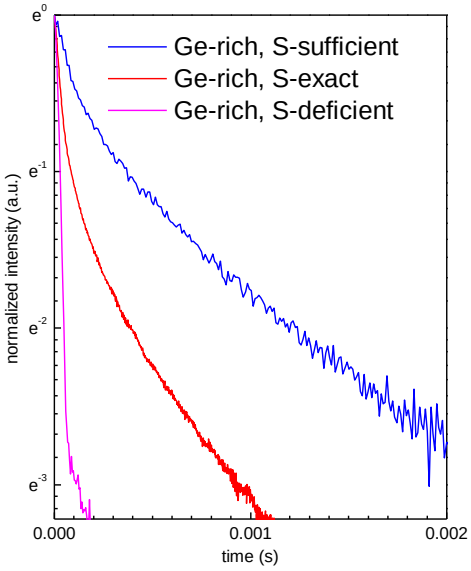

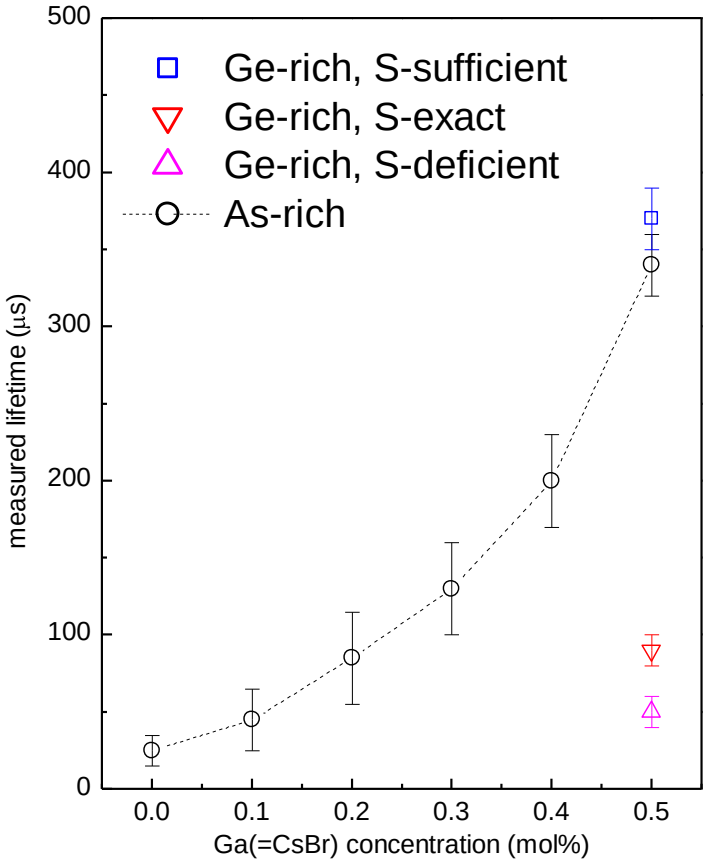

* Choi et al, J. Appl. Phys. 98 (2005) 023523.

Host sensitization of RE^{3+} emission

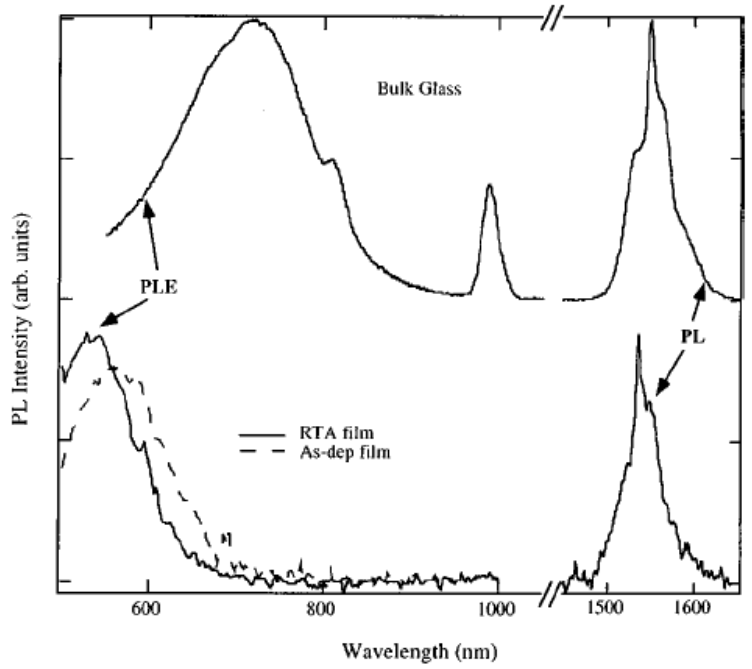

FIG. 1. Room temperature PL and PLE spectra obtained from 0.5 wt. % Er:$Ge_{33}As_{12}Se_{55}$ bulk glass and 1-μm-thick sputtered films of 0.5 wt. % Er:$Ge_{10}As_{40}S_{25}Se_{25}$ glass. PL spectra were excited by a tungsten lamp operating at 700 nm for the bulk glass and 560 nm for the films. The excitation spectrum ''blue shifts'' due to RTA of the films.

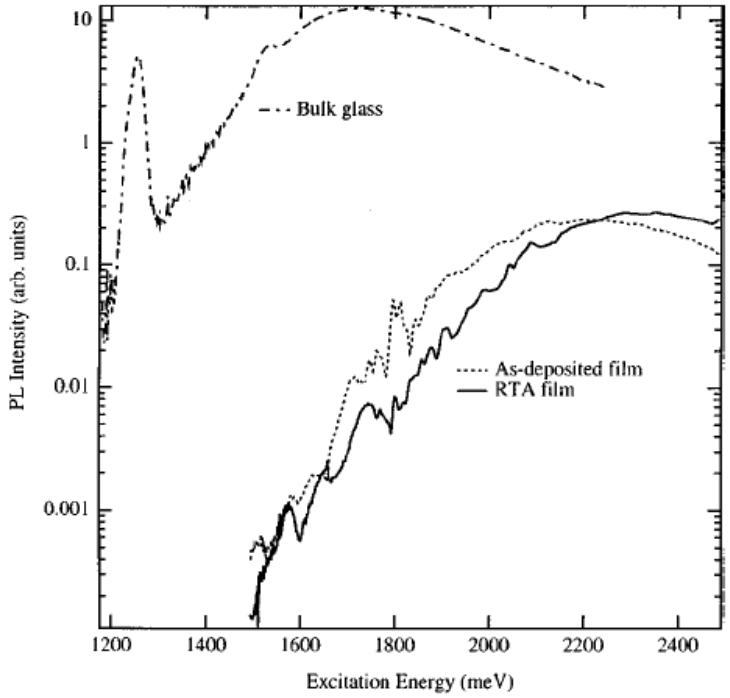

FIG. 2. Semilogarithmic, excitation photon energy scale representation of the room temperature PLE spectra shown in Fig. 1. Low energy ranges of all three PLE spectra exhibit exponential increases, characteristic of the Urbach absorption edge in chalcogenide glasses. The intensity of the bulk spectrum is arbitrarily offset from that of the films for clarity.

- ✓ Proposed mechanism;
  - ➢ Optical absorption in the Urbach edge of the host glass
  - ➢ Carrier localization at native defects in the glass
  - ➢ Subsequent nonradiative energy transfer from the defects to the RE atoms.
- ✓ What about photo-darkening?

* Ramachandran and Bishop, Appl. Phys. Lett. 73 (1998) 3196.

V-doped Ga-La-S glass

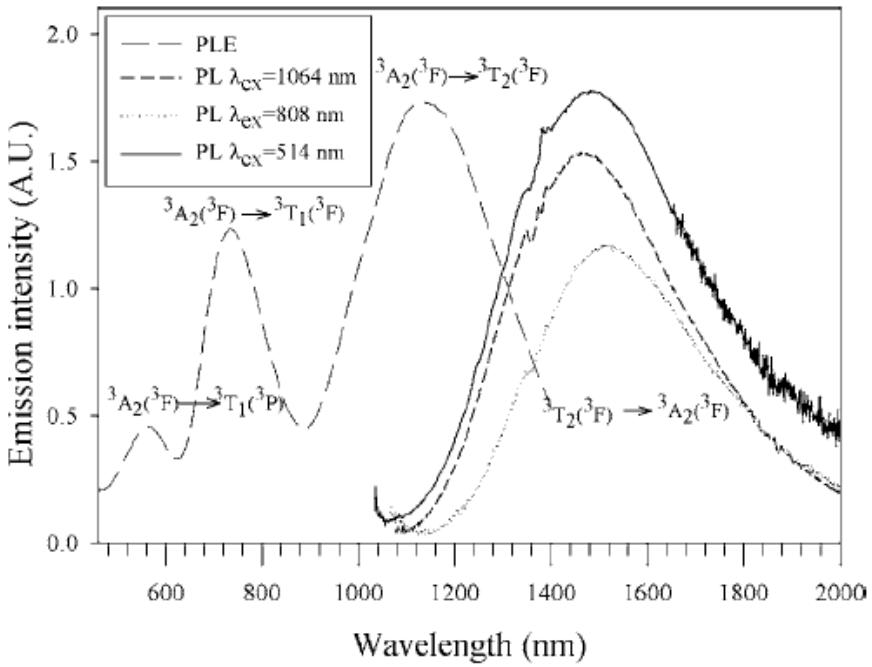

FIG. 2. Excitation and photoluminescence spectra of 0.01% vanadium doped GLS.

TABLE I. Overview of the spectroscopic parameters for various laser materials compared to V:GLS.

Ion:Host	τ (μs)	η_{QE} (%)	σ_{em} (10^{-2} cm^2)	$\sigma_{em}\tau$ (10^{-24} s cm^2)	Ref.
V^{3+}:GLS	33	4	0.03	0.1	This work
$Cr^{4+}:Y_2SiO_5$	1.3	<10	2.0	0.26	24
$Cr^{4+}:YAl_5O_{12}$	4.1	22	3.3	1.35	25
$V^{2+}:MgF_2$	40		0.08	0.32	26
$Ti^{3+}:Al_2O_3$	3.1	100	4.5	1.40	27

* Hughes et al, Appl. Phys. Lett. 90 (2007) 031108.

Bi-doped Ga-La-S glass

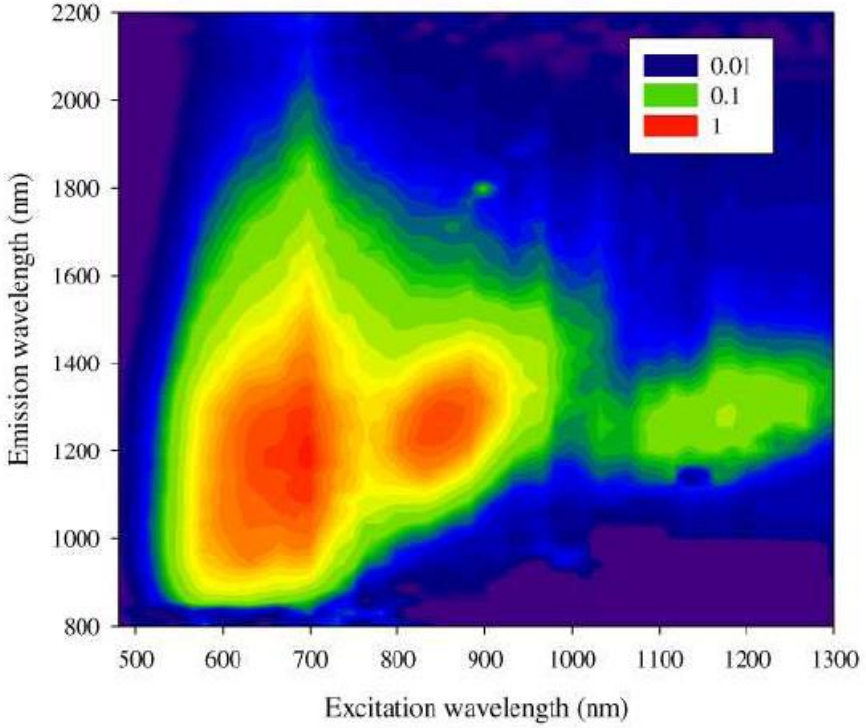

Fig. 2. Contour plot showing the emission spectra, normalized to the excitation power, of Bi doped GLS at excitation wavelengths of 480-1300 nm. Emission intensity is in a log scale.

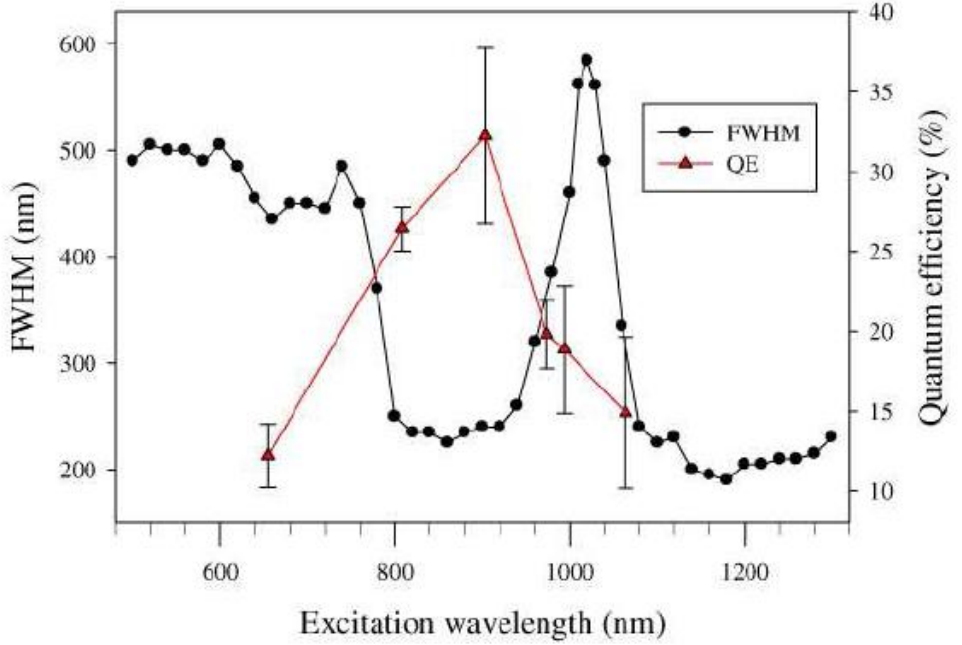

Fig. 3. Emission FWHM and quantum efficiency as a function of excitation wavelength.

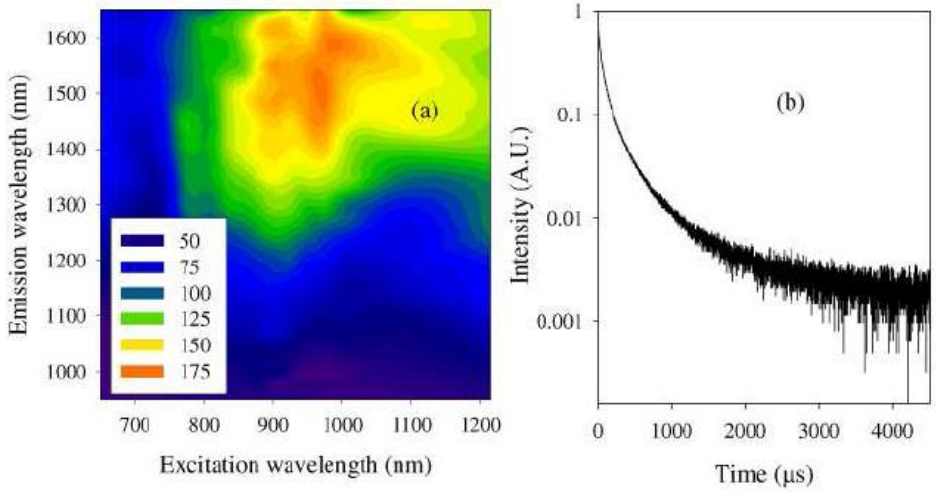

Fig. 7. Room temperature lifetime (μs) as a function of excitation and emission wavelength (a). Example of an emission decay (b).

"By examining previously published models of Bi emission in glasses to see if they could account for the 2000 and 2600 nm emission bands we suggest that the origin of the emission in Bi:GLS is $(Bi_2)^{2-}$ dimers."

* Hughes et al, Optics Express, 17 (2009) 19345.

What of Bi results in the emission?

Surprisingly, the nature of this NIR photoluminescence is still unknown, although many hypotheses have been formulated, attributing emission to Bi^{5+} [37–40], Bi-clusters [17], Bi^{+} [22,23,25,26,28,34,35], BiO [8,31,41], dimer ions Bi_2, Bi_2^- and Bi_2^{2-} [11,12,24,42], Bi^0 [43,44], molecular orbital models [40,45,46] or even point defects [21]. In the present paper, all these attempts to clarify the origin of NIR emission will be critically evaluated with the goal to condense the accumulated information into a potential resolution of the problem, and to identify directions for future research.

The various hypotheses appeared in the chronological order: (1) Bi^{5+} (Fujimoto and Nakatsuka [37]), (2) bismuth in lower valency (Peng et al. [3]), (3) Bi^{+} (Meng et al. [22,23]), (4) Bi-clusters (Peng et al. [17]), (5) BiO (Ren et al. [41]), (6) Bi_2^-/Bi_2 (Khonthon et al. [11]), (7) Bi_2^-/Bi_2^{2-} (Sokolov et al. [42]), (8) point defects (Sharonov et al. [21]), (9) Bi^0 (Peng et al. [43]), (10) intramolecular charge transfer in $Bi^{5+}O_n^{2-}$ molecules (Kustov et al. [45,46]), and (11) radiative recombination of e–h pairs in $Bi^{5+}O_n^{2-}$ molecules (Razdobreev et al. [40]). We categorize these into three groups: (A) bismuth in higher valency, i.e. Bi^{5+} and related molecules; (B) bismuth in lower valency, i.e. BiO, Bi^{+}, Bi^0, cluster ions; and (C) point defects. Emphasis will be on the first two groups.

* Peng et al, J. Non-Cryst. Solids, (2010) in press.